


Article

Enhanced Reactive Power Sharing and Voltage Restoration Based on Adaptive Virtual Impedance and Consensus Algorithm

Mohamed Keddar ^{1,*}, Mamadou Lamine Doumbia ¹, Karim Belmokhtar ² and Mohamed Della Krachai ³ 

¹ Department of Electrical and Computer Engineering, Université du Québec à Trois-Rivières, Trois-Rivières, QC G8Z 4M3, Canada; mamadou.doumbia@uqtr.ca

² Research and Innovation, Nergica, Gaspé, QC G4X 1G2, Canada; kbelmokhtar@nergica.com

³ Department of Electrical Engineering, University of Science and Technology Mohamed Boudiaf, Oran 31000, Algeria; mohamed.dellakrachai@univ-usto.dz

* Correspondence: mohamed.keddar@uqtr.ca

Abstract: In this paper, power-sharing management control on an AC islanded microgrid is investigated to achieve accurate reactive power sharing. The droop control method is primarily used to manage the active and reactive power sharing among the DGs in the microgrid. However, the line impedance mismatch causes unbalanced reactive power sharing. As a solution a consensus-based adaptive virtual impedance controller is proposed, where the consensus algorithm is used to set the reactive power mismatch; then a virtual impedance correction term is generated through a proportional-integral controller to eliminate the line impedance mismatch. Thus, reactive power sharing is achieved without knowledge of the line impedances or using a central controller. Moreover, the consensus algorithm is used to restore the AC bus voltage to the nominal value by estimating the DGs average voltage using neighbor communication to compensate for the decreased magnitude of the voltage reference. Matlab/Simulink is used to validate the accuracy of reactive power sharing and voltage restoration achievement of the proposed solution through simulation of different scenarios. In addition, a dSPACE DS1104 is used within a developed experimental testbench based on two parallel DGs to validate the effectiveness of the proposed solution in the real world.

Keywords: consensus control; virtual impedance; microgrids; distributed generation; dSPACE controller; droop control



Citation: Keddar, M.; Doumbia, M.L.; Belmokhtar, K.; Krachai, M.D. Enhanced Reactive Power Sharing and Voltage Restoration Based on Adaptive Virtual Impedance and Consensus Algorithm. *Energies* **2022**, *15*, 3480. <https://doi.org/10.3390/en15103480>

Academic Editor: Ferdinanda Ponci

Received: 4 April 2022

Accepted: 3 May 2022

Published: 10 May 2022

Publisher's Note: MDPI stays neutral with regard to jurisdictional claims in published maps and institutional affiliations.



Copyright: © 2022 by the authors. Licensee MDPI, Basel, Switzerland. This article is an open access article distributed under the terms and conditions of the Creative Commons Attribution (CC BY) license (<https://creativecommons.org/licenses/by/4.0/>).

1. Introduction

The world energy demand is increasing quickly, and it is expected to reach 50% by 2050 [1]. This is due to the increase in the population of the world and the rapid development of technologies. To accommodate this growth in energy demand, the development of new power generation and massive integration of renewable energy become a priority respecting the agreements on the emission reduction of CO₂. Recently, several new technologies have been contributing to power generation plants such as the Distributed Generation (DG) using renewable energy sources, Electrolyzers (Ely) and fuel cells (FC), Electric Vehicles (EVs), and Energy Storage Systems (ESSs). Connected to a common bus with a centralized or decentralized controller and power management system with communication, they establish a new power generation system called a microgrid (MG). A MG can operate in both connected mode when it is coupled to the main grid, or autonomous mode when it is islanded [2,3].

The massive integration of Renewable Energy Resources (RES) in MGs can reduce the operation cost, increase the benefits on the environment by reducing the CO₂ emissions, and create new power sources [4]. However, the nature of these sources and sudden variations in the weather cause perturbation and instability to the MG, resulting in voltage

and frequency deviations. MGs are considered to have a low system inertia due to the low capacity of the DGs supplied by RES. Furthermore, the sudden changes in the connected loads may lead to critical frequency deviations and power flow management issues during the MG operation [5–7].

In autonomous microgrids, the connected DGs share the load power according to their power ratings for the profitability and to ensure the stability of the MG. The commonly adopted method in power sharing is the droop control approach. Active power sharing between DGs can be easily achieved using the frequency droop control method, whereas the reactive power sharing cannot be achieved easily due to the impedance mismatch between DGs which leads to voltage deviation and system instability [8,9]. To solve the inaccurate reactive power sharing issue, other ameliorated control methods have been developed [10–13]. In [10], a decentralized self-changing control was proposed using the adaptive droop control method. To increase the accuracy of reactive power sharing, an inductive virtual impedance (VI) loop was introduced; however, this method was not examined for a wide scope of working points. In [11], an adaptive droop controller was proposed to ensure dynamic stability of power sharing, where derivatives of active and reactive power are added to the traditional droop controller. Then, droop control gains were tuned adaptively conforming to the output power variations. However, the reactive power sharing was not as expected [12]. A modified Q-V droop control method was introduced in [13] to improve the power sharing accuracy. However, the reactive power sharing difference cannot be completely removed.

Other methods based on improved hierarchical control strategies have been proposed [14,15]. A secondary controller with a primary droop controller was presented in [14] to achieve accurate reactive power sharing in islanded MGs. However, a communication link between the central controller (CC) and DG's local controller is needed, increasing the response time and the total cost. In [15], virtual impedance control was applied in islanding MGs at different levels according to transient variations in the active power. A transient control term was used in the traditional droop control by injecting frequency disturbances. However, this approach could result in lower reliability and instability of the MG because of their reliance on the central controller. Moreover, the reactive power sharing was not addressed. Nonetheless, in these methods, power-sharing accuracy, especially reactive power can be influenced by communication congestion or delays regarding the number of connected DGs [16,17]. VI-based methods were widely used to improve reactive power sharing [18–20]. The VI is used to eliminate the impedance mismatch between lines and then improve reactive power sharing as well system stability. Based on injection of disturbances, online impedance estimation, or using MGCC, this approach can flexibly deal with the impedance mismatch between lines as well as the variation in load power, improving the dynamic performance of the MG. In order to enhance accurate reactive power sharing between parallel DGs, a complex VI approach including resistive and inductive factors systems was introduced [21,22] where the reactive power sharing was significantly enhanced. Furthermore, the result can be better with communication-based complex VI [23]. However, the communication delays can result in less reactive power sharing accuracy and degraded performance.

Recently, consensus algorithms were combined with the adaptive VI approach in order to guarantee accurate power sharing and current harmonics sharing. In addition, the voltage and the frequency value restoration can be achieved using these algorithms. Based on the information from neighbor communication or MGCC systems, the consensus approach is used to guarantee accurate reactive power distribution. The virtual impedance of DGs is tuned by the consensus approach to move towards a common objective in terms of reactive power sharing [24–26]. However, the communication system should be optimized to enhance the MG stability and improve the MG performance.

When only the neighbor communication system is used, the MG cost and communication time will be reduced. This kind of communication can be used in one or two directions, depending on the system specifications. Reactive current information can be used in order

to have accurate reactive power sharing. On the other hand, the active current information is used for active power sharing accuracy [27]. Moreover, to compensate for the voltage deviations and drop caused by the VI, DG output voltage restoration was introduced using a consensus algorithm [23]. The approach uses a communication system between adjacent DGs to exchange information on reactive power sharing and voltage restoration. However, this approach is dependent on communication system reliability. Microgrid reliability and efficiency are related to several parameters such as communication links and control strategy. MGCC presents a very sturdy and efficient control strategy. However, the complex communication system may increase the total cost as well as the impact of communication time delays. Therefore, decentralized control strategies are favored especially in autonomous MG where DGs, loads, and storage systems are from multiple customers. In this case, complex central communication systems should be avoided in order to reduce the information dependency on each DG.

Encouraged by this aspect, several attempts have been made by this work. Since the reactive power sharing issue is directly related to the DGs voltage and their behaviors, it can be solved based on information exchange between adjacent DGs and local information through a progressive process. The line impedance can be first estimated and tuned by each DG using the consensus algorithm; then this value can be shared with the neighbors. The VI is adaptively adjusted by the consensus algorithm to remove the mismatch between line impedance, ensuring accurate reactive power sharing without line impedance knowledge. Furthermore, the consensus control is used to compensate and restore the output voltage of each DG to the MG voltage. Therefore, the developed control contributions from this work are summarized as follows:

Adaptive virtual impedance control combined with a consensus algorithm is proposed for reactive power-sharing accuracy and parallel DGs voltage restoration with line impedance mismatch in autonomous MGs.

To achieve accurate reactive power sharing, neighbor information through a unidirectional communication link is used to estimate the VI, reducing the cost and the time delay impact of communication. Additionally, this approach cancels out the line impedance knowledge.

The proposed control approach was confirmed by experimental validation using a small-scale laboratory test bench based on MGs with two DGs.

The rest of the paper is arranged as follows: Section 2 presents the power sharing using conventional droop, the microgrid configuration, control, and modeling. Section 3 explores the proposed approach based on adaptive VI and consensus algorithms used to have accurate reactive power sharing and system voltage restoration. Then, Section 4 shows the simulation verification and Section 5 presents the experimental validation results of the proposed control approach. Finally, summary and main findings of this paper are presented in Section 6.

2. Droop Control and Reactive Power Sharing Theory

Droop control is the most used classical approach to control parallel DGs in power systems. This method presents high flexibility with good reliability and redundancy. It does not require a central controller or communication system and is mostly used in the primary control of MGs.

2.1. Droop Control

To analyze the power flow in steady state, it is assumed that the inverter is a controlled voltage source; then the dynamics of the inner control loop can be neglected. Figure 1 illustrates an inverter connected to the point of common coupling (PCC) through a line impedance Z .

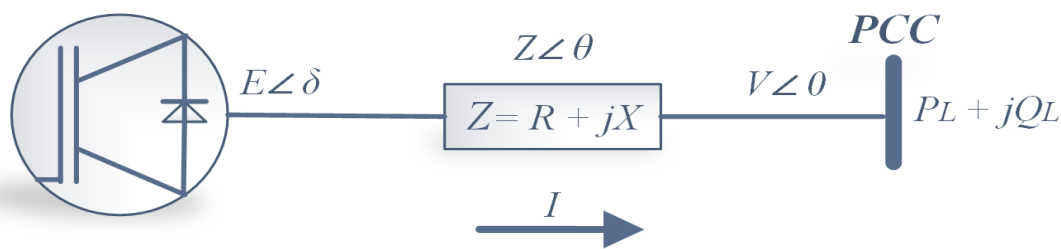


Figure 1. Inverter connected the point of common coupling.

Assuming a balanced 3-phase system, the power flowing in a transmission line can be derived by:

$$S = P + jQ = V * I = E * \left(\frac{E - V}{Z} \right) \tag{1}$$

$$S \equiv \frac{P}{E} + j \frac{Q}{E} = \frac{E - V}{Z} * e^{j(\theta + \delta)} \tag{1}$$

where S, Q, P represent apparent, reactive, and active power, respectively. E represents the output voltage of the power inverter at an angle δ . Z represents the impedance of the transmission line between the inverter and the PCC with angles V and θ that represent the voltage at the PCC with an angle equal to zero. Using Euler's simplification and replacing the line impedance by $Z = R + jX$, the active and reactive power equations can be written as follows [28]:

$$Q = \frac{E}{X^2 + R^2} (X(E - V \cos \delta) + RV \sin \delta) \tag{2}$$

$$P = \frac{E}{X^2 + R^2} (R(E - V \cos \delta) + XV \sin \delta) \tag{3}$$

In normal cases, the output power of a DG unit is far below the maximum transmission capability of the feeder line; thus, δ will be small. For this reason, the approximation $\cos \delta \rightarrow 1$ and $\sin \delta \rightarrow \delta$ can be adopted. In addition, assuming that the line impedance is inductive and satisfies the condition $X^2 \gg R^2$ Equations (2) and (3) become:

In normal cases, the output power of a DG unit is far below the maximum transmission capability of the feeder line; thus, δ will be small. For this reason, the approximation $\cos \delta \rightarrow 1$ and $\sin \delta \rightarrow \delta$ can be adopted. In addition, assuming that the line impedance is inductive and satisfies the condition $Xi \gg Ri$ Equations (2) and (3) become:

$$E - V \cong \frac{XQ}{E} \tag{4}$$

Equations (4) and (5) show that the power angle strongly depends on the active power and the voltage difference depends on the reactive power. In other words, active power can be frequency controlled and reactive power regulated by voltage. This finding leads to the following common droop control equations:

Equations (4) and (5) show that the power angle strongly depends on the active power and the voltage difference depends on the reactive power. In other words, active power can be frequency controlled and reactive power regulated by voltage. This finding leads to the following common droop control equations:

where V_0 and ω_0 , represent the nominal values of the voltage and the frequency, n_Q and m_P represent the droop coefficients, and V, ω , represent the nominal output of the voltage and the frequency. Then, the droop control coefficients (n_Q, m_P) can be defined by the following equations [28,29]:

$$V = V_0 - n_Q Q \tag{7}$$

where V_0 and ω_0 , represent the nominal values of the voltage and the frequency, n_Q and m_P represent the droop coefficients, and V, ω , represent the nominal output of the voltage and the frequency. Then, the droop control coefficients (n_Q, m_P) can be defined by the following equations [28,29]:

$$n_Q = \frac{\Delta \omega_{max}}{Q_{nominal}} \tag{9}$$

$$m_p = \frac{\Delta\omega_{max}}{P_{nominal}} \tag{8}$$

$$n_q = \frac{\Delta v_{max}}{Q_{nominal}} \tag{9}$$

2.2.2. Reactive Power Sharing

Accurate reactive power sharing cannot be achieved by conventional droop control. In order to solve the issue and eliminate the deviations of the voltage and frequency, secondary control was used. Fig. 2 shows the investigated MG configuration in a case of distributed generation (DG) based renewable energy sources and battery storage systems (BSS). Each DG is connected to a common AC bus through an inverter and an LCL filter.

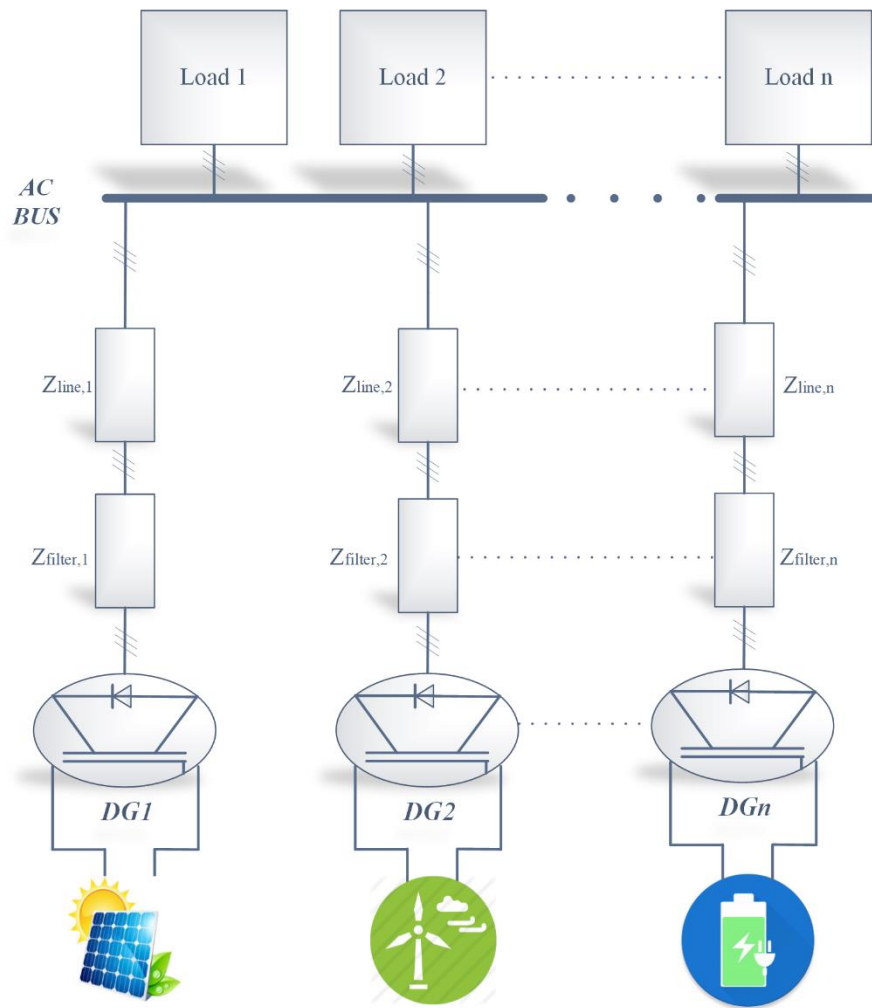


Figure 2. Configuration of the investigated islanded microgrid.

The control structure of the MG is based on hierarchical control using primary and secondary control levels. The primary control contains the current and voltage control loops. While the secondary control contains the consensus algorithm, adaptive virtual impedance, and droop control.

2.3. DGs Modeling and Global Control Strategy

The control strategy at the primary control level is based on proportional-integral (PI) controllers. Figure 3 shows the global control scheme of inverters for each DG. Secondary control level includes the droop controller, power calculation, the adaptive virtual impedance, and the consensus algorithm with the communication network. References of voltage and adaptive VI value are generated and sent to the primary control level. Afterward, inverter control signals are generated based on these references. An LCL filter is used to connect the inverter to the AC bus, where L_f is the inverter side inductor of the

The control strategy at the primary control level is based on proportional-integral (PI) controllers. Figure 3 shows the global control scheme of inverters for each DG. Secondary control level includes the droop controller, power calculation, the adaptive virtual impedance, and the consensus algorithm with the communication network. References of voltage and adaptive VI value are generated and sent to the primary control level. Afterward, inverter control signals are generated based on these references. An LCL filter is used to connect the inverter to the AC bus, where L_f is the inverter side inductor of the filter with R_f as internal resistance, C_f is the capacitor value of the filter and finally, L_g is the inductor of the filter at the grid side with an internal resistance R_g .

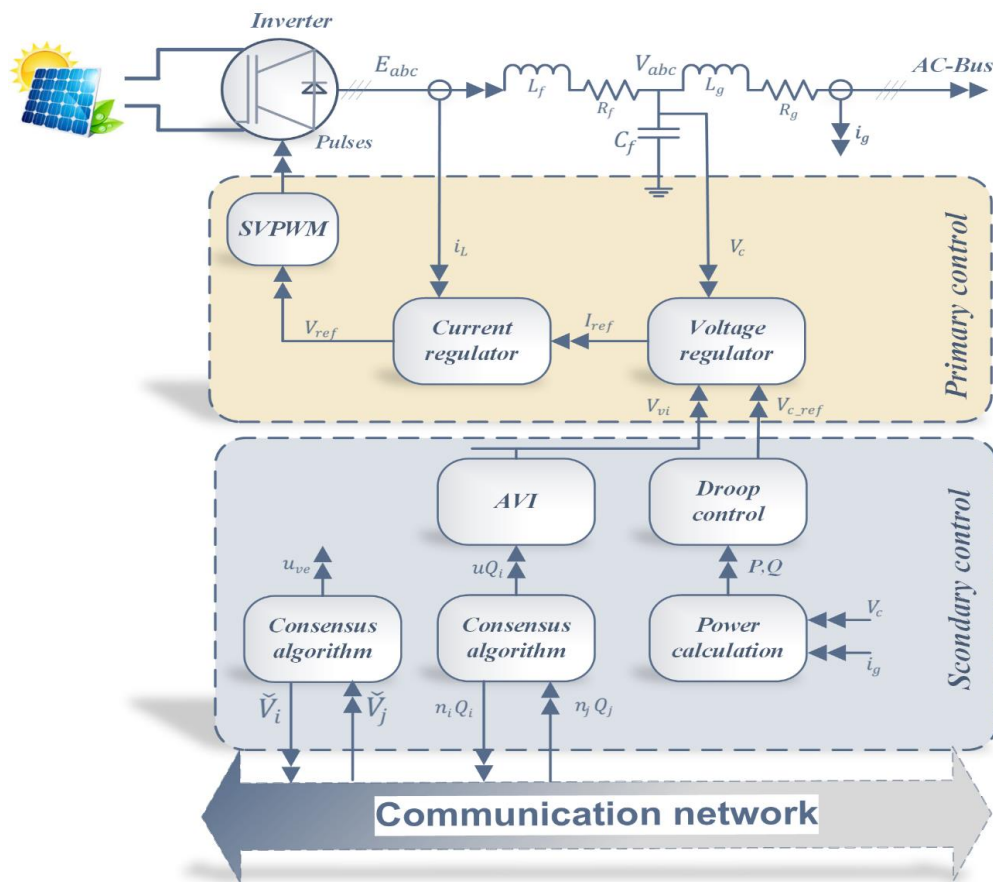


Figure 3. Global control scheme of DGs.

The dynamic equations model can be derived using voltage and current law followed by Park transformation as follows:

$$L_f * \frac{d}{dt} \begin{bmatrix} i_d \\ i_q \end{bmatrix} = \begin{bmatrix} E_d \\ E_q \end{bmatrix} - \begin{bmatrix} v_d \\ v_q \end{bmatrix} - R_f \begin{bmatrix} i_d \\ i_q \end{bmatrix} + \begin{bmatrix} \omega L_f i_q \\ -\omega L_f i_d \end{bmatrix} \quad (10)$$

$$C_f * \frac{d}{dt} \begin{bmatrix} v_d \\ v_q \end{bmatrix} = \begin{bmatrix} i_d \\ i_q \end{bmatrix} - \begin{bmatrix} i_d \\ i_q \end{bmatrix} + \begin{bmatrix} 0 & \omega C_f \\ -\omega C_f & 0 \end{bmatrix} \begin{bmatrix} v_d \\ v_q \end{bmatrix} \quad (11)$$

where E_d, E_q represent direct and quadrature voltage before the filter, V_d, V_q after the filter, and i_d, i_q the current direct and quadrature values. After simplification, the equations of the current and the voltage controllers can be written as follows [2]:

$$\begin{cases} I_{ref_d} = (K_{pv} + \frac{K_{iv}}{s})(V_{cdref*} - V_{cd}) - \omega C V_{cq} + i_{gq} \\ I_{ref_q} = (K_{pv} + \frac{K_{iv}}{s})(V_{cqref*} - V_{cq}) - \omega C V_{cd} + i_{gd} \end{cases} \quad (12)$$

$$\begin{cases} V_{ref_d} = (K_{pi} + \frac{K_{ii}}{s})(i_{ref_d} - i_{id}) - \omega L_f i_{iq} + V_{cq} \\ V_{ref_q} = (K_{pi} + \frac{K_{ii}}{s})(i_{ref_q} - i_{iq}) - \omega L_f i_{id} + V_{cd} \end{cases} \quad (13)$$

where K_{pi}, K_{ii} are the proportional and the integral coefficients of the current PI controller, K_{pv}, K_{iv} are the proportional and the integral coefficients of the voltage PI controller. V_{cdref*}

and V_{cqref*} are the voltage references calculated by the droop controller. The adaptive VI control is as follows:

$$\begin{bmatrix} V_{cdref*} \\ V_{cqref*} \end{bmatrix} = \begin{bmatrix} V_{c_refd} - V_{vi_d} \\ V_{c_refq} - V_{vi_q} \end{bmatrix} \quad (14)$$

where V_{vi_d} , V_{vi_q} represent the references from the adaptive VI controller and V_{c_refd} , V_{c_refq} the references of the droop controller.

3. Adaptive Virtual Impedance and Consensus Algorithm

In a MG, the active and reactive power are coupled and depend on the output frequency and voltage due to the nature of the line impedance, which can be resistive inductive or both. The use of VI in combination with the physical impedance can modify the total output impedance of the DG. In this section, the proposed approach based on adaptive VI and consensus algorithms is explored.

3.1. Adaptive Virtual Impedance

VI has been used for many applications recently, such as reactive power sharing by ensuring a consistent and equivalent output impedance for all parallel DGs in the autonomous MGs [2,25–27]. This VI can be adjusted adaptively in order to calculate the total impedance and then the voltage reference. Thus, the total output impedance of a DG can be written as follows [27]:

$$Z_i = Z_{line,i} + Z_{v,i} + Z_{adp,i} \quad (15)$$

Z_i represents the total output impedance of the DG_{*i*} and the line impedance can be represented by $Z_{line,i}$. The virtual impedance can be divided into two terms, $Z_{v,i}$ which represents the static virtual impedance value used to ensure an inductive total impedance. The other term, $Z_{adp,i}$ represents the adaptive VI. Equation (15) shows that the output impedance of each DG is increased by the adaptive term in order to match with other DG impedances and eliminate the mismatch. Then, reactive power sharing can be improved using droop control relations.

3.2. Consensus Algorithm

In order to have a similar output impedance between different DGs, in this work, the adaptive VI in Equation (14) is calculated and adjusted using a consensus algorithm. To have an accurate reactive power sharing, consensus control is used to reach a general agreement among all MG agents. Thus, the droop control and reactive power coefficients must be designed to be inversely proportional, according to the following equation [26–29]:

$$n_{Q1}Q_1 = n_{Q2}Q_2 = \dots = n_{QN}Q_N \quad (16)$$

By replacing (7) in (5), the reactive power flow of each DG can be written as follows:

$$n_{qi}Q_i = \frac{V(E_0 - V)}{\frac{X_i}{n_i} + V} \quad (17)$$

Therefore, to satisfy Equation (16), the term X_i/n_i of each DG must be the same in Equation (17), from which the following equation can be written:

$$\frac{X_1}{n_1} = \frac{X_2}{n_2} = \dots = \frac{X_N}{n_N} \quad (18)$$

From Equation (18), it can be noticed that the term n_i must be proportional to the line reactance X_i . Considering Equation (16), in order to obtain accurate reactive power sharing the reactance of the line must be designed to be inversely proportional to the reactive power, then the following equation can be written [23,25,26]:

$$X_1 Q_1 = X_2 Q_2 = \dots = X_N Q_N \tag{19}$$

The consensus control of the reactive power can be treated as a synchronization problem of a first-order linear agent system [26–28]. Then, Equation (20) is obtained from the linearization of Equation (15):

$$u_{Q_i} = n_{Q_i} \dot{Q}_i = -C_{nQ} e_{niQ_i} \tag{20}$$

where, u_{Q_i} is the auxiliary control, e_{niQ_i} represents the reactive power error between the local DG and its neighbor, and C_{nQ} is the coupling gain. The local neighbor’s reactive power sharing error is represented by:

$$e_{niQ_i} = \sum_{j=N} a_{ij} (n_{Q_i} Q_i - n_{Q_j} Q_j) \tag{21}$$

where a_{ij} represents the changes in connection between DGs from the adjacency matrix. The whole consensus system can be written in matrix representation as:

$$\begin{bmatrix} u_{Q_1} \\ u_{Q_1} \\ \vdots \\ u_{Q_N} \end{bmatrix} = \begin{bmatrix} n_{Q_1} \dot{Q}_1 \\ n_{Q_2} \dot{Q}_2 \\ \vdots \\ n_{Q_N} \dot{Q}_N \end{bmatrix} = - \begin{bmatrix} n_{Q_1} \dot{Q}_1 \\ n_{Q_2} \dot{Q}_2 \\ \vdots \\ n_{Q_N} \dot{Q}_N \end{bmatrix} * \sum_{j=N} \begin{bmatrix} a_{1j} \\ a_{2j} \\ \vdots \\ a_{Nj} \end{bmatrix} * \begin{bmatrix} (n_{Q_1} Q_1 - n_{Q_j} Q_j) \\ (n_{Q_2} Q_2 - n_{Q_j} Q_j) \\ \vdots \\ (n_{Q_N} Q_N - n_{Q_j} Q_j) \end{bmatrix} \tag{22}$$

Then the Adaptive VI references in Equation (14) can be presented as follows:

$$\begin{bmatrix} V_{vi_d} \\ V_{vi_q} \end{bmatrix} = \begin{bmatrix} R_{vi} & -\omega L_{vi} \\ R_{vi} & \omega L_{vi} \end{bmatrix} \begin{bmatrix} i_{gd} \\ i_{gq} \end{bmatrix} \tag{23}$$

$$\begin{bmatrix} L_{vi} \\ R_{vi} \end{bmatrix} = \begin{bmatrix} L_{vi}^* \\ R_{vi}^* \end{bmatrix} - u_{Q_i} \begin{bmatrix} k_l \\ k_r \end{bmatrix} \tag{24}$$

where, L_{vi}^* and R_{vi}^* represent the resistance and inductance of the static impedance. L_{vi} and R_{vi} are the resistance and inductance of the VI. k_l and k_r are adjusting gains of the consensus controller. Based on these equations, the adaptive VI implementation is illustrated in Figure 4.

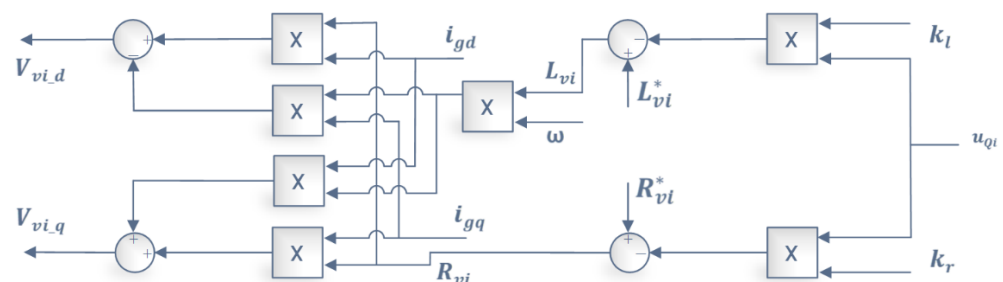


Figure 4. Adaptive VI and consensus algorithm implementation.

3.3. Bus Voltage Restoration

In order to compensate the voltage drop caused by the droop control and the VI, a secondary voltage compensation based voltage compensation is used. The average voltage of each DG to the MG based on the average voltage of the average voltage between DGs to the MG nominal voltage. This will eliminate the voltage of the MG. The average voltage of the DG can be defined as the average output voltage value of all MG DGs [23,26,27]:

$$\check{V} = \sum_{j=1}^N \frac{V_j}{N} \tag{25}$$

$$\check{V} = \sum_{j=1}^{Nj=1} \frac{V_j}{N} \tag{25}$$

where \check{V} is the average voltage, V_j is the output voltage of DG_i , and N is the total number of DGs connected to the MG. Using the consensus based adaptive VI control, once the virtual impedance is adaptively set and the reactive power sharing is achieved, the droop

$$\check{V} = \sum_{j=1}^N \frac{V_j}{N} \tag{25}$$

where \check{V} is the average voltage, V_j is the output voltage of DG_j , and N is the total number of DGs. \check{V} is the average voltage. Using the output voltage of DG_i and N is the total number of DGs connected to the MG. Using the consensus based sliding mode control, the droop control and the virtual impedance is adaptively adjusted to the reactive power. However, the droop control the output voltage of each DG generated has a fixed. However, the DG output voltage at the filter output level, cannot be identical for all the DGs due to inductance and mismatch in the cable resistance. This can cause deviations in the output voltage and exceed the allowable range. Therefore, a secondary control for voltage restoration should be used to regulate the average MG voltage. The DG level for voltage restoration can be expressed using its own output voltage \check{V}_i and its neighbor DG voltage \check{V}_j .

$$\check{V}_i(t) = \check{V}_i(\bar{t}) + \frac{C_v}{C_p} \int_0^t \sum_{j \in n_{ij}, j \neq i} g_{ij} (\check{V}_j(\bar{t}) - \check{V}_i(\bar{t})) dt \tag{26}$$

where V_i is the voltage of DG_i and C_v is a coupling gain. Then, the dynamics of the voltage where V_i is the voltage of DG_i and C_v is a coupling gain. Then, the dynamics of the voltage consensus control can be expressed as follows:

$$\dot{\check{V}}_i(\bar{t}) = \check{V}_i(\bar{t}) + C_p \sum_{j \in n_{ij}, j \neq i} g_{ij} (\check{V}_j(\bar{t}) - \check{V}_i(\bar{t})) \tag{27}$$

The implementation of the proposed approach for voltage restoration is shown in Figure 5:

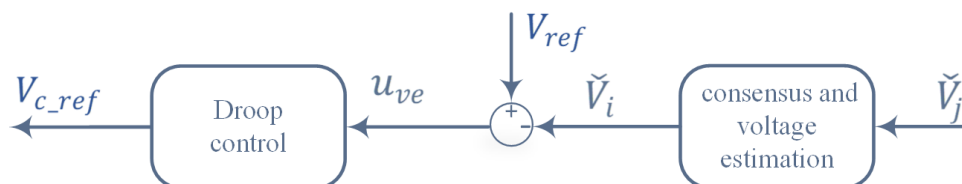


Figure 5. Implementation of the reference voltage generator.

4. Simulation Verification

In order to verify the effectiveness of the proposed control approach, simulation tests were conducted using MATLAB/Simulink software. The MG shown in Figure 2 was modeled in Simulink. The MG is composed of three DGs connected to renewable energy sources (solar or wind) with different rated powers and a battery storage system. All DGs are connected to the AC bus through an LCL filter and an impedance. Moreover, different loads are connected to the AC bus. All DGs are connected to a communication link in order to change information between neighbors. The sharing power ratio is 1:1:0.5 for DG1, DG2, and DG3, respectively. Table 1 shows the parameters used in this simulation. The simulation is divided into three parts. In the first one, reactive power sharing accuracy was verified using the proposed control approach. In the second one, the robustness of the control approach under load changes is explored, and finally, in the third one, the voltage restoration performance was investigated.

Table 1. Simulation parameters.

Parameters	Value
Inverter power rating	5 KVA
Line voltage	208 V
Bus frequency	60 Hz
Dc bus voltage	400 V
Line impedances	
line 1	7.5 mH, 0.6 Ω
line 2	4.5 mH, 0.5 Ω
line 3	7.5 mH, 0.6 Ω
Proportional gain in PI current controller K_{pi}	50
Integral gain in PI current controller K_{ii}	0.5

Table 1. Cont.

Parameters	Value
Proportional gain in PI voltage controller Kpv	2
Integral gain in PI voltage controller Kiv	0.5
Droop coefficient	
mP1, mP2	2×10^{-4}
mP3	4×10^{-4}
nQ1, nQ2	5×10^{-4}
nQ3	7.5×10^{-4}
Load 1	4 kW, 1.1 kVAR
Load 2	2.2 kW, 0.6 kVAR
Load 3,4	1 kW, 0.25 kVAR

4.1. Case Study #1

Figure 6 represents the active power sharing between the three DGs. The active power was well shared before and after applying the proposed strategy. The reactive power sharing is shown in Figure 7, where it is not achieved using the conventional method. The proposed control strategy was applied at $t = 7.5$ s, which offers an accurate reactive power sharing in the desired ratio without affecting the active power sharing. The virtual resistance and reactance of each DG are illustrated in Figures 8 and 9.

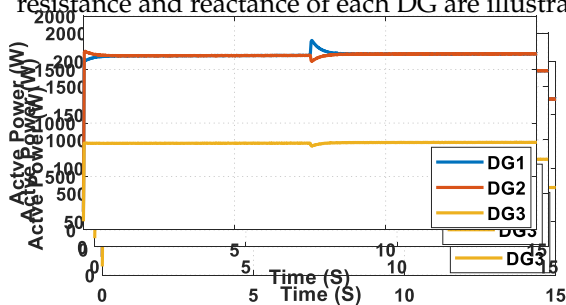


Figure 6. Active power of DGs.

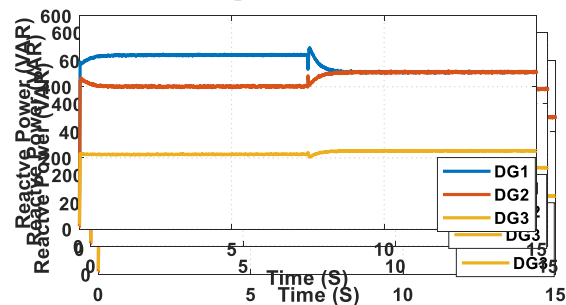


Figure 7. Reactive power of DGs.

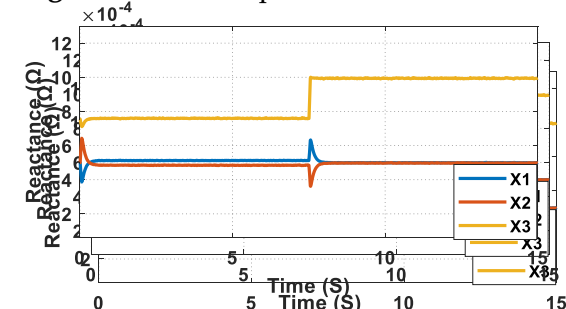
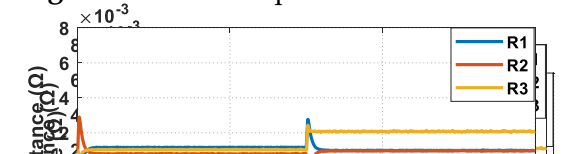


Figure 8. Virtual impedance reactance.



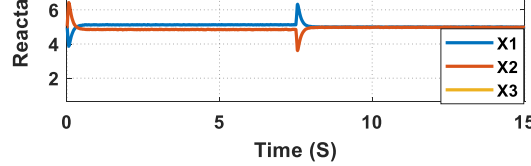


Figure 8. Virtual impedance reactance.

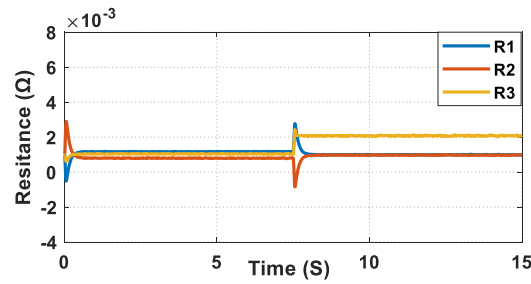


Figure 9. Virtual impedance resistances.

After activating the consensus algorithm control, DG1 and 2 resistance and reactance values become equal. This is due to their equal power-sharing ratios. While the resistance and reactance values for DG3 are larger because the sharing ratio of this DG is lower than the others.

In the second part of the simulations, the performance of the system was tested during load changes. In this case study, the renewable resources are operated under de-loaded mode, their maximum output power is between $t = 5$ s and $t = 7.5$ s. Otherwise, they are operated under three DGs currents. After $t = 7.5$ s, the output currents of DGs become synchronized and proportional to the nominal power demanded by loads and the phases are almost identical.

Before the application of the proposed method, there was a phase shift between the three DGs currents. After $t = 7.5$ s, the output currents of DGs become synchronized and proportional to the nominal power demanded by loads and the phases are almost identical.

Initially, the system load is (2.2 kW, 0.6 kVAR), after $t = 2.5$ s, the load was increased to (3.2 kW, 0.85 kVAR), then after $t = 5$ s, the load was increased to (4.2 kW, 1.1 kVAR). Finally, at $t = 7.5$ s the load was reduced to (3.2 kW, 0.85 kVAR). The simulation results are shown in Figures 11–14. For active and reactive power sharing and by Figure 11, the consensus control eliminates progressively the reactive power error between DGs during all periods of load changes, as shown by these results.

As can be seen that the current values are well synchronized and proportional to the power demand of each DG. The same was reflected on all load change conditions during this simulation period. The changes during simulation are represented in Figure 14.

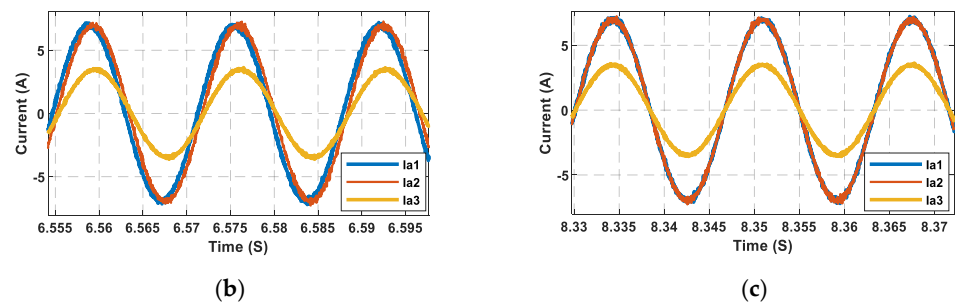


Figure 10. Output currents of DGs, (a) output current, (b) zoom before, and (c) zoom after applying the proposed controller.

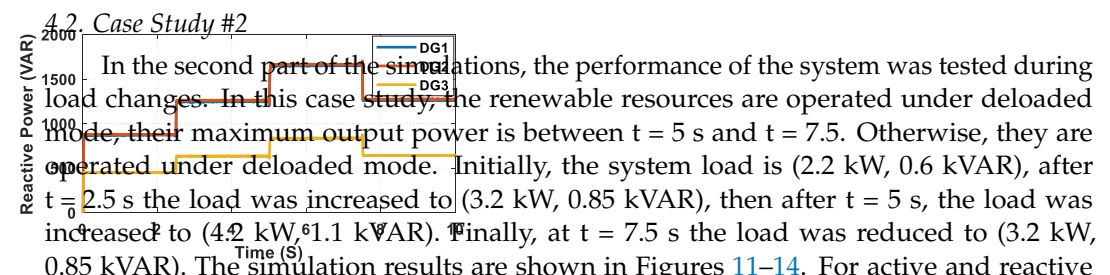


Figure 11. Active power sharing of DGs.

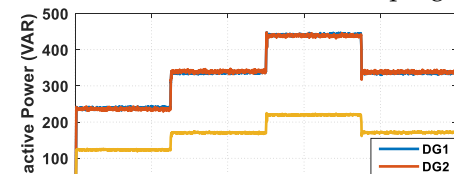


Figure 12. Reactive power error of DGs.

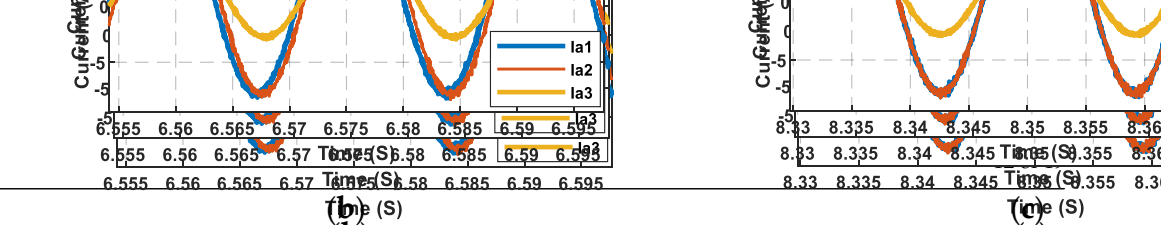


Figure 10. Output currents of DGs. (a) output current, (b) zoom before, and (c) zoom after. The proposed controller provides better performance than the proposed controller. The proposed controller provides better performance than the proposed controller. The proposed controller provides better performance than the proposed controller.

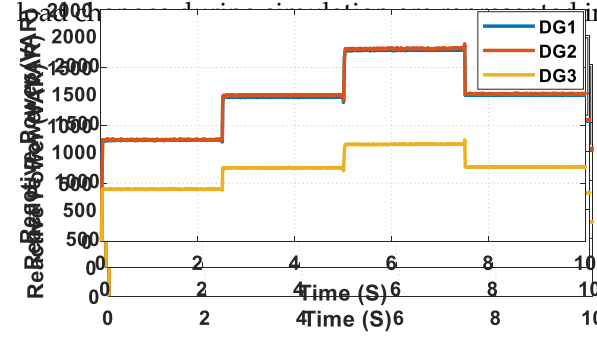


Figure 11. Active power of DGs.

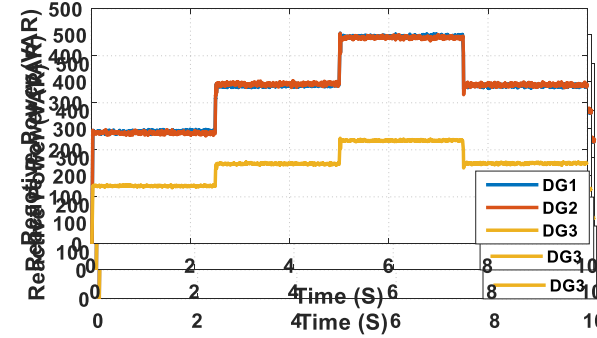


Figure 12. Reactive power of DGs.

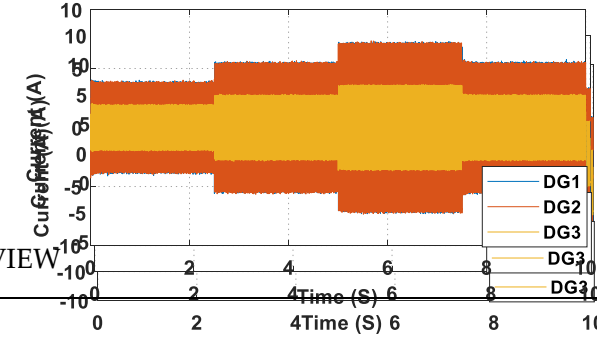


Figure 13. Output current of DGs.

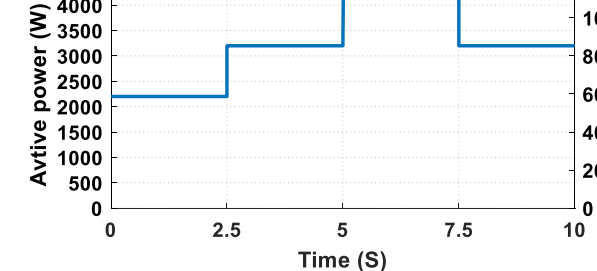


Figure 14. Load profile.

4.3. Case Study #3

The third simulation case was dedicated to voltage restoration controlling, one load was connected to the AC bus, then at time $t = 1.5$ s the rest was activated. To verify the effectiveness of the voltage restoration control

Figure 14. Load profile.
 4.3. Case Study #3
 4.3. Case Study #3
 4.3. Case Study #3

The third simulation case was dedicated to voltage restoration control. The load was connected to the AC bus, then at time $t = 1.5$ s the restoration control was activated. To verify the effectiveness of the voltage restoration control, one load was connected to the AC bus, then at time $t = 1.5$ s the restoration control was activated to verify the effectiveness of the voltage restoration control. The results of this simulation are shown in Figure 15. Initially, the output voltages of the three DGs are lower than the reference voltage. After application of the proposed control (at $t = 1.5$ s), the output voltages of the three DGs increased and converged to the reference voltage. The active and reactive power sharing was always maintained, as shown in Figure 16 and Figure 17. After application of the proposed control (at $t = 1.5$ s), the active and reactive power sharing was always maintained, as shown in Figure 16 and Figure 17. The output frequency was maintained within the range of 50 Hz. The average voltage of the AC bus was always maintained at 120 V. Figure 18 shows the average voltage of the AC bus. The latter was maintained at 120 V. Figure 19 shows the output frequency was maintained within the range of 50 Hz. Figure 20 shows the average voltage of the AC bus. The latter was maintained at 120 V. Figure 21 shows the active power of the three DGs. The active power of each DG was always maintained at its nominal value. Figure 22 shows the reactive power of the three DGs. The reactive power of each DG was always maintained at its nominal value. The changes during simulation are represented in Figure 21. The load changes during simulation are represented in Figure 22.

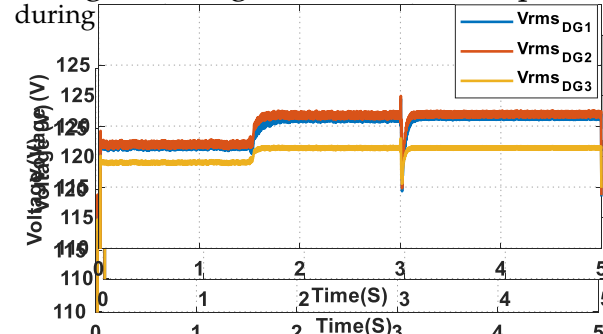


Figure 15. Output voltage of DGs.
 Figure 15. Output voltage of DGs.
 Figure 15. Output voltage of DGs.

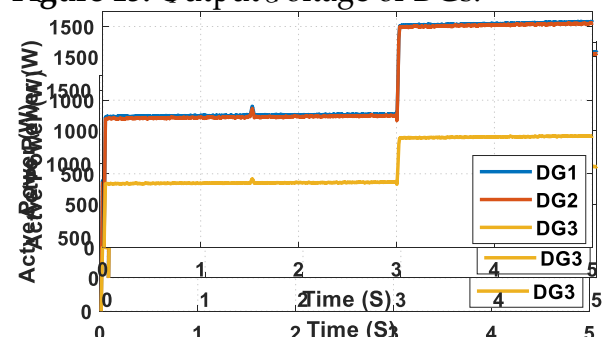


Figure 16. Active power of DGs.
 Figure 16. Active power of DGs.
 Figure 16. Active power of DGs.

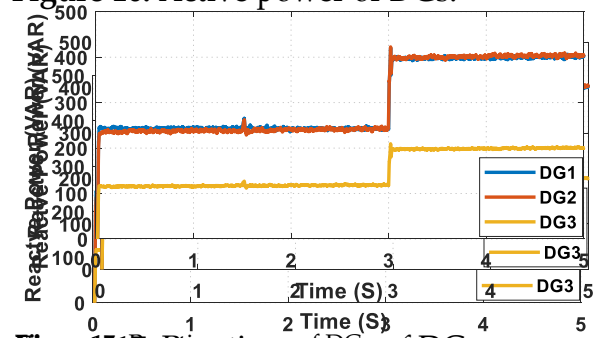


Figure 17. Reactive power of DGs.
 Figure 17. Reactive power of DGs.
 Figure 17. Reactive power of DGs.

the line impedances. Finally, two inductive resistive loads are connected to the AC bus through contactors to allow connection or disconnection of these loads. The experimental parameters are illustrated in Table 2 and the benchmark is shown in Figure 22.

Table 2. Experimental parameters

Parameters		Value	
Power rating		500 VA	
Line voltage		Value	40 V
Bus frequency		500 VA	60 Hz
DC bus voltage		40 V	80 V
Bus frequency		60 Hz	
DC bus voltage		80 V	
Line impedances		0.82 mH, 0.02 Ω	
line 1			
line 2		0.82 mH, 0.03 Ω	
Proportional gain in PI current controller	Kpi	1.2 mH, 0.03 Ω	100
Integral gain in PI current controller	Kii	100	0.5
Proportional gain in PI voltage controller	Kpv	0.5	50
Integral gain in PI voltage controller	Kiv	50	1.5
Droop coefficient			
mP1	mP1	2×10^{-3}	2×10^{-3}
mP2	mP2	4×10^{-3}	4×10^{-3}
nQ1	nQ1,	5×10^{-3}	5×10^{-3}
nQ2	nQ2	7.5×10^{-3}	7.5×10^{-3}

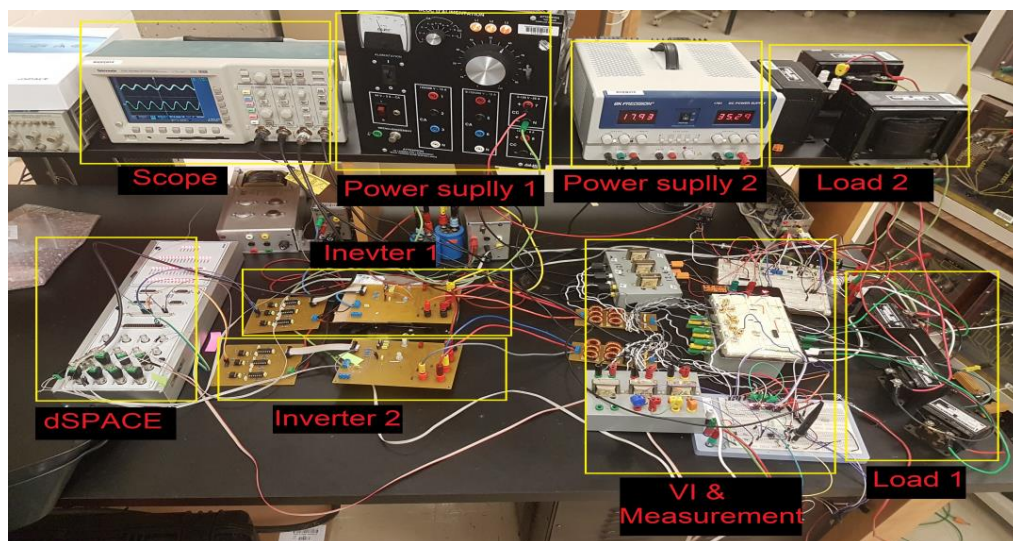


Figure 22. Laboratory experimental benchmark.

5511. Case Study #1

The first scenario of experimental validation was carried out to verify the sharing of active and reactive power. The power sharing used in these tests is that shown in the Fig. 23. Figure 23 shows the active power well shared between the two inverters, before the application of the proposed approach. The reactive power sharing is shown in Figure 24. Figure 24 has not achieved using the conventional method. The application of the proposed control strategy after which allowed a reactive power sharing. The outputs of inverter are shown in Figure 25, Figure 26, Figure 27, and Figure 28. The output current of inverter is shown in Figure 29. The output voltage of inverter is shown in Figure 30. The output power of inverter is shown in Figure 31. The output power of inverter is shown in Figure 32. The output power of inverter is shown in Figure 33. The output power of inverter is shown in Figure 34. The output power of inverter is shown in Figure 35. The output power of inverter is shown in Figure 36. The output power of inverter is shown in Figure 37. The output power of inverter is shown in Figure 38. The output power of inverter is shown in Figure 39. The output power of inverter is shown in Figure 40. The output power of inverter is shown in Figure 41. The output power of inverter is shown in Figure 42. The output power of inverter is shown in Figure 43. The output power of inverter is shown in Figure 44. The output power of inverter is shown in Figure 45. The output power of inverter is shown in Figure 46. The output power of inverter is shown in Figure 47. The output power of inverter is shown in Figure 48. The output power of inverter is shown in Figure 49. The output power of inverter is shown in Figure 50. The output power of inverter is shown in Figure 51. The output power of inverter is shown in Figure 52. The output power of inverter is shown in Figure 53. The output power of inverter is shown in Figure 54. The output power of inverter is shown in Figure 55. The output power of inverter is shown in Figure 56. The output power of inverter is shown in Figure 57. The output power of inverter is shown in Figure 58. The output power of inverter is shown in Figure 59. The output power of inverter is shown in Figure 60. The output power of inverter is shown in Figure 61. The output power of inverter is shown in Figure 62. The output power of inverter is shown in Figure 63. The output power of inverter is shown in Figure 64. The output power of inverter is shown in Figure 65. The output power of inverter is shown in Figure 66. The output power of inverter is shown in Figure 67. The output power of inverter is shown in Figure 68. The output power of inverter is shown in Figure 69. The output power of inverter is shown in Figure 70. The output power of inverter is shown in Figure 71. The output power of inverter is shown in Figure 72. The output power of inverter is shown in Figure 73. The output power of inverter is shown in Figure 74. The output power of inverter is shown in Figure 75. The output power of inverter is shown in Figure 76. The output power of inverter is shown in Figure 77. The output power of inverter is shown in Figure 78. The output power of inverter is shown in Figure 79. The output power of inverter is shown in Figure 80. The output power of inverter is shown in Figure 81. The output power of inverter is shown in Figure 82. The output power of inverter is shown in Figure 83. The output power of inverter is shown in Figure 84. The output power of inverter is shown in Figure 85. The output power of inverter is shown in Figure 86. The output power of inverter is shown in Figure 87. The output power of inverter is shown in Figure 88. The output power of inverter is shown in Figure 89. The output power of inverter is shown in Figure 90. The output power of inverter is shown in Figure 91. The output power of inverter is shown in Figure 92. The output power of inverter is shown in Figure 93. The output power of inverter is shown in Figure 94. The output power of inverter is shown in Figure 95. The output power of inverter is shown in Figure 96. The output power of inverter is shown in Figure 97. The output power of inverter is shown in Figure 98. The output power of inverter is shown in Figure 99. The output power of inverter is shown in Figure 100.

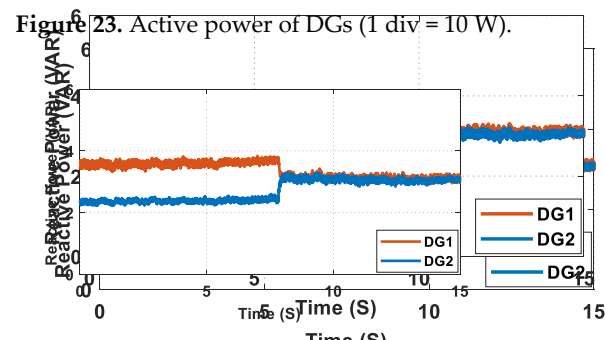
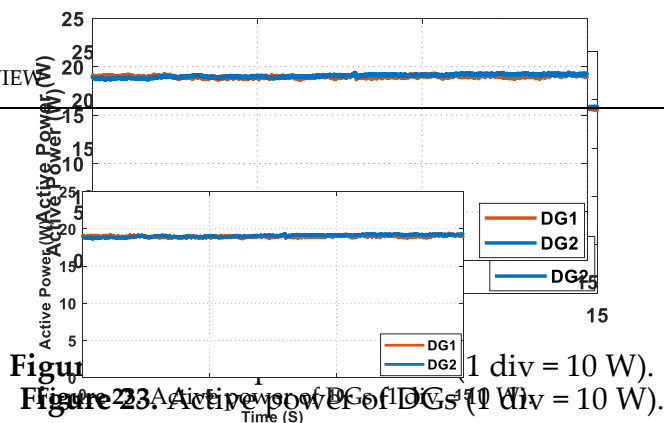


Figure 23. Active power of DGs (1 div = 10 W).
 Figure 24. Reactive power of DGs (1 div = 10 VAR).

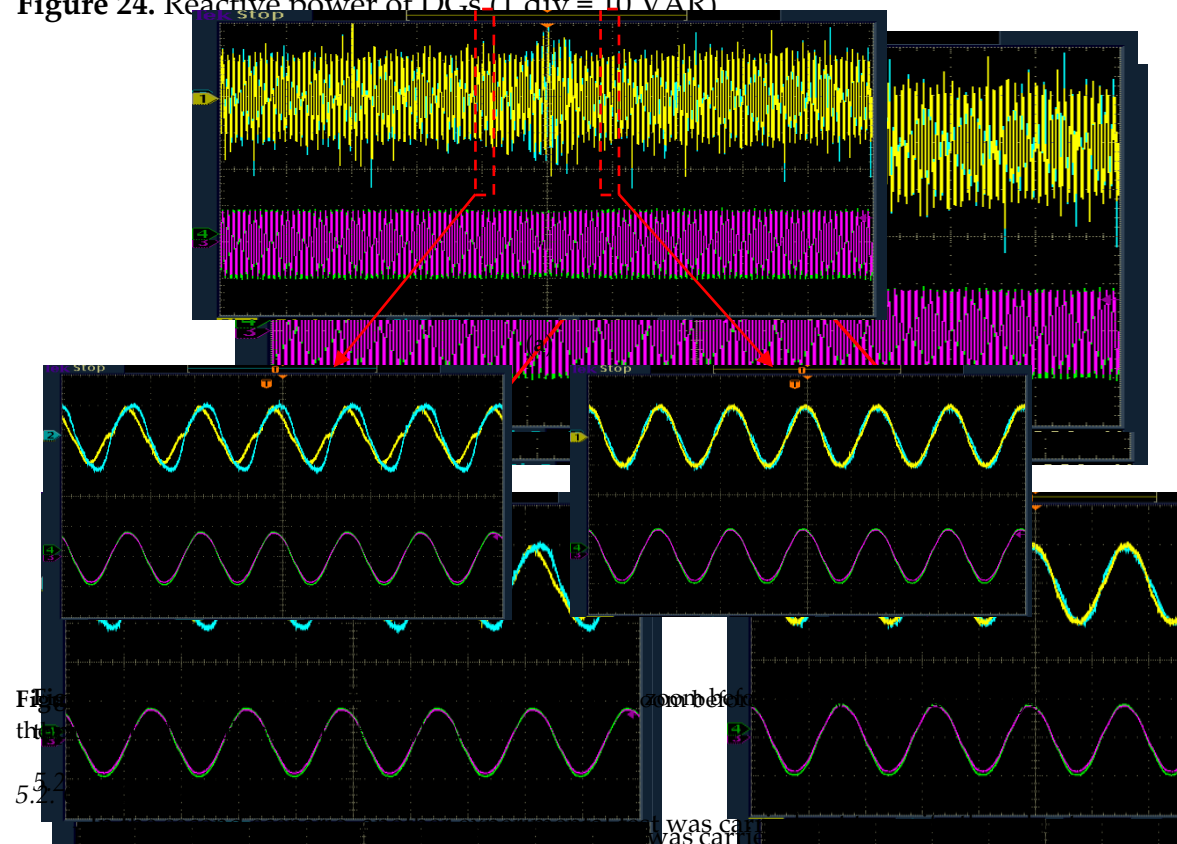


Figure 25. Output currents of DGs and the active and reactive power shared between DGs. (a) shows the active power of DG1, (b) shows the active power of DG2, (c) shows the reactive power of DG1, and (d) shows the reactive power of DG2. The load was increased from 1280 W, 30 VAR to 3880 W, 60 VAR at time $t = 10$ s. As expected, the results are similar to the simulation, both DGs follow the change and the active and reactive power was shared accordingly as shown in Figures 26 and 27, respectively. Figure 28 shows the voltage of the load, a slight drop was observed when the load increases. Figure 29 shows the load changes during simulation. The output currents of each DG are shown in Figure 30 at the 5.2 s. The currents are well synchronized with the same amplitude, then increase when the load increases. In the second scenario, another experimental test was carried out to verify the proposed approach by increasing load. The load was increased from 1280 W, 30 VAR to 3880 W, 60 VAR at time $t = 10$ s. As expected, the results are similar to the simulation, both DGs follow the change and the active and reactive power was shared accordingly as shown in Figures 26 and 27, respectively. Figure 28 shows the voltage of the load, a slight drop was observed when the load increases. Figure 29 shows the load changes during simulation. The output currents of each DG are shown in Figure 30 at the 5.2 s. The currents are well synchronized with the same amplitude, then increase when the load increases. In the second scenario, another experimental test was carried out to verify the proposed approach by increasing load. The load was increased from 1280 W, 30 VAR to 3880 W, 60 VAR at time $t = 10$ s. As expected, the results are similar to the simulation, both DGs follow the change and the active and reactive power was shared accordingly as shown in Figures 26 and 27, respectively. Figure 28 shows the voltage of the load, a slight drop was observed when the load increases. Figure 29 shows the load changes during simulation. The output currents of each DG are shown in Figure 30 at the 5.2 s. The currents are well synchronized with the same amplitude, then increase when the load increases.

top. The currents are well synchronized with the same amplitude, then increase when the load rises, while the DGs output voltage keeps the same value as shown in the same figure at the bottom. This confirms the effectiveness of the PLL and droop control with the same RMS value. Figure 26 shows the active power of the DGs. The active power of the DGs is 100 W. Figure 27 shows the reactive power of the DGs. They are well synchronized with the same RMS value. Figure 28 shows the output voltage of the DGs. They are well synchronized with the same RMS value. Figure 29 shows the load profile. Figure 30 shows the output current of the DGs.

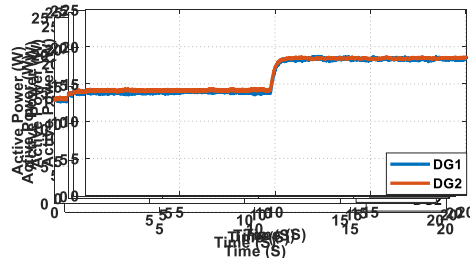


Figure 26. Active power of DGs ($P_{dg} = 100\text{ W}$).

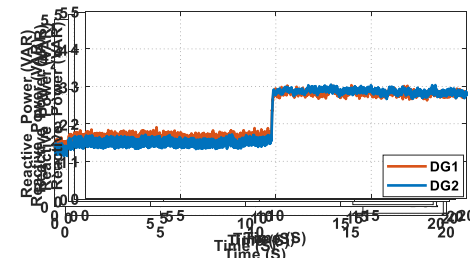


Figure 27. Reactive power of DGs ($P_{dq} = 100\text{ VAR}$).

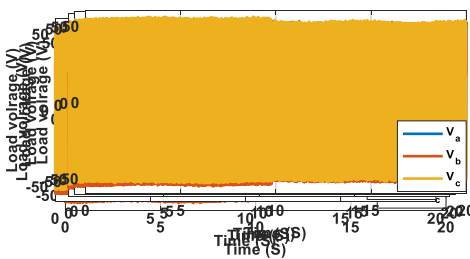


Figure 28. Output voltage of DGs.

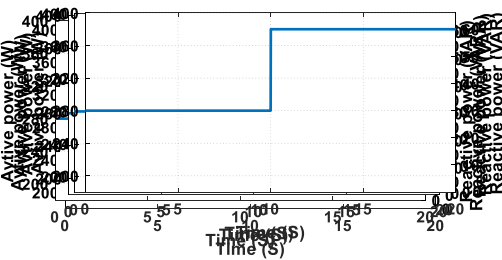


Figure 29. Load profile.

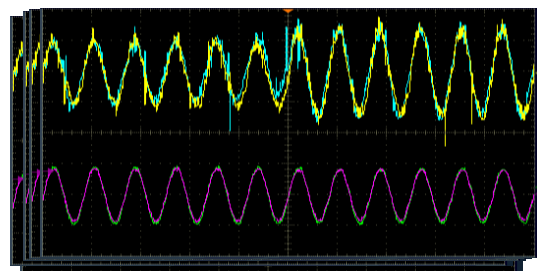


Figure 30. Output current of DGs ($I_{dg} = 5\text{ A}/500\text{ W}$).

6. Kerdphol, T.; Rahman, F.S.; Mitani, Y.; Watanabe, M.; Kufeoglu, S. Robust Virtual Inertia Control of an Islanded Microgrid Considering High Penetration of Renewable Energy. *IEEE Access* **2018**, *6*, 625–636. [[CrossRef](#)]
7. Ma, D.; Liu, M.; Zhang, H.; Wang, R.; Xie, X. Accurate power sharing and voltage regulation for AC microgrids: An event-triggered coordinated control approach. *IEEE Trans. Cybern.* **2021**, 1–11. [[CrossRef](#)] [[PubMed](#)]
8. Raj, D.C.; Gaonkar, D.N. Frequency and voltage droop control of parallel inverters in microgrid. In Proceedings of the 2016 2nd International Conference on Control, Instrumentation, Energy & Communication (CIEC), Kolkata, India, 28–30 January 2016; pp. 407–411.
9. Bouzid, A.E.; Sicard, P.; Yamane, A.; Paquin, J.N. Simulation of droop control strategy for parallel inverters in autonomous AC microgrids. In Proceedings of the 2016 8th International Conference on Modelling, Identification and Control (ICMIC), Algiers, Algeria, 15–17 November 2016; pp. 701–706.
10. Hamzeh, M.; Mokhtari, H.; Karimi, H. A decentralized self-adjusting control strategy for reactive power management in an islanded multi-bus MV microgrid. *Can. J. Electr. Comput. Eng.* **2013**, *36*, 18–25. [[CrossRef](#)]
11. Mohamed, Y.; El-Saadany, E.F. Adaptive decentralized droop controller to preserve power sharing stability of paralleled inverters in distributed generation microgrids. *IEEE Trans. Power Electron.* **2008**, *23*, 2806–2816. [[CrossRef](#)]
12. Mahmood, H.; Michaelson, D.; Jiang, J. Reactive power sharing in islanded microgrids using adaptive voltage droop control. *IEEE Trans. Smart Grid* **2015**, *6*, 3052–3060. [[CrossRef](#)]
13. Zhou, J.; Cheng, P. A Modified Q–V Droop Control for Accurate Reactive Power Sharing in Distributed Generation Microgrid. *IEEE Trans. Ind. Appl.* **2019**, *55*, 4100–4109. [[CrossRef](#)]
14. He, J.; Li, Y.W.; Blaabjerg, F. Voltage Stability and Reactive Power Sharing in Review of Active and Reactive Power Sharing Strategies in Hierarchical Controlled Microgrids. *IEEE Trans. Power Electron.* **2015**, *30*, 3389–3401. [[CrossRef](#)]
15. Micallef, A.; Apap, M.; Staines, C.S.; Guerrero, J.M. Secondary Control for Reactive Power Sharing in Droop-Controlled Islanded Microgrids. In Proceedings of the 3rd IEEE International Symposium on Power Electronics for Distributed Generation Systems (PEDG), Aalborg, Denmark, 25–28 June 2012; pp. 492–498.
16. Han, Y.; Li, H.; Shen, P.; Coelho, E.A.A.; Guerrero, J.M. Review of active and reactive power sharing strategies in hierarchical controlled microgrids. *IEEE Trans. Power Electron.* **2017**, *32*, 2427–2451. [[CrossRef](#)]
17. Schiffer, J.; Seel, T.; Raisch, J.; Sezi, T. Voltage Stability and Reactive Power Sharing in Inverter-Based Microgrids With Consensus-Based Distributed Voltage Control. *IEEE Trans. Control Syst. Technol.* **2016**, *24*, 96–109. [[CrossRef](#)]
18. Zhu, Y.; Zhuo, F.; Wang, F.; Liu, B.; Gou, R.; Zhao, Y. A virtual impedance optimization method for reactive power sharing in networked microgrid. *IEEE Trans. Power Electron.* **2016**, *31*, 2890–2904. [[CrossRef](#)]
19. Mahmood, H.; Michaelson, D.; Jiang, J. Accurate reactive power sharing in an islanded microgrid using adaptive virtual impedances. *IEEE Trans. Power Electron.* **2015**, *30*, 1605–1617. [[CrossRef](#)]
20. He, J.; Li, Y.W.; Guerrero, J.M.; Vasquez, J.C.; Blaabjerg, F. An islanding microgrid reactive power sharing scheme enhanced by programmed virtual impedances. In Proceedings of the 3rd IEEE International Symposium on Power Electronics for Distributed Generation Systems (PEDG), Aalborg, Denmark, 25–28 June 2012; pp. 229–235.
21. Hoang, T.V.; Lee, H.H. An Adaptive Virtual Impedance Control Scheme to Eliminate the Reactive-Power-Sharing Errors in an Islanding Meshed Microgrid. *IEEE J. Emerg. Sel. Top. Power Electron.* **2017**, *6*, 966–976. [[CrossRef](#)]
22. Zandi, F.; Fani, B.; Sadeghkhan, I.; Orakzadeh, A. Adaptive complex virtual impedance control scheme for accurate reactive power sharing of inverter interfaced autonomous microgrids. *IET Gener. Trans. Distrib.* **2018**, *12*, 6021–6032. [[CrossRef](#)]
23. Zhang, H.; Kim, S.; Sun, Q.; Zhou, J. Distributed adaptive virtual impedance control for accurate reactive power sharing based on consensus control in microgrids. *IEEE Trans. Smart Grid* **2017**, *8*, 1749–1761. [[CrossRef](#)]
24. An, R.; Liu, Z.; Liu, J. Successive-approximation-based virtual impedance tuning method for accurate reactive power sharing in islanded microgrids. *IEEE Trans Power Electron.* **2020**, *36*, 87–102. [[CrossRef](#)]
25. Yu, L.; Shi, D.; Xu, G.; Guo, X.; Jiang, Z.; Jing, C. Consensus Control of Distributed Energy Resources in a Multi-Bus Microgrid for Reactive Power Sharing and Voltage Control. *Energies* **2018**, *11*, 2710. [[CrossRef](#)]
26. Alsafran, A.S.; Daniels, M.W. Consensus Control for Reactive Power Sharing Using an Adaptive Virtual Impedance Approach. *Energies* **2020**, *13*, 2026. [[CrossRef](#)]
27. Lyu, Z.; Wei, Q.; Zhang, Y.; Zhao, J.; Manla, E. Adaptive Virtual Impedance Droop Control Based on Consensus Control of Reactive Current. *Energies* **2018**, *11*, 1801. [[CrossRef](#)]
28. Sultani, J.F. *Modelling, Design and Implementation Of D-Q Control in Single-Phase Grid-Connected Inverters for Photovoltaic Systems Used in Domestic Dwellings*; De Montfort University: Leicester, UK, 2013.
29. Keddar, M.; Doumbia, M.L.; Belmokhtar, K.; Della Krachai, M. Experimental Validation of an Accurate Reactive Power-Sharing Approach Based on Adaptive Virtual Impedance and Consensus Control. In Proceedings of the 12th International Renewable Energy Congress (IREC), Hammamet, Tunisia, 26–28 October 2021; pp. 1–6.